ELSEVIER

Journal of Organometallic Chemistry 637–639 (2001) 586–594

Journal of Organometallic Chemistry

www.elsevier.com/locate/jorganchem

A re-examination of the reaction between 1,1′-bis(diphenylphosphino)ferrocene (dppf) diselenide and $[Ru_3(CO)_{12}]$. Electrochemical behaviour of the isomeric *nido*-clusters $[Ru_3(\mu_3\text{-}Se)_2(dppf)(CO)_7]$ and $[Ru_3(\mu_3\text{-}Se)_2(\mu\text{-}dppf)(CO)_7]$ and crystal structure of $[Ru_3Se\{\mu\text{-}P(Ph)C_5H_4FeC_5H_4PPh_2\}(\mu\text{-}OCPh)(CO)_6]$

Fabrizia Fabrizi de Biani [a], Claudia Graiff [b], Giuliana Opromolla [a], Giovanni Predieri [b,*], Antonio Tiripicchio [b], Piero Zanello [a,*]

[a] *Dipartimento di Chimica, Università di Siena, Via Aldo Moro, 53100 Siena, Italy*
[b] *Dipartimento di Chimica G.I.A.F., Università di Parma, Centro S.S.D. del C.N.R., Parco Area delle Scienze, 43100 Parma, Italy*

Received 7 February 2001; received in revised form 5 March 2001; accepted 24 April 2001

Abstract

The reactions of 1,1′-bis(diphenylphosphino)ferrocene diselenide (dppfSe2) with $[Ru_3(CO)_{12}]$ at 60 and 110 °C afford, respectively, the two isomeric *nido*-clusters $[Ru_3(\mu_3\text{-}Se)_2(dppf)(CO)_7]$ (**2**) and $[Ru_3(\mu_3\text{-}Se)_2(CO)_7(\mu\text{-}dppf)]$ (**3**) which contain dppf as chelating and bridging ligand, respectively. The chelated derivative **2**, attainable under kinetic control, can be converted to the more stable bridged cluster **3** by thermal treatment in toluene solution. Moreover the cluster $[Ru_3Se\{\mu\text{-}P(Ph)C_5H_4FeC_5H_4PPh_2\}(\mu\text{-}OCPh)(CO)_6]$ (**4**) was isolated as a minor product. Its cluster core consists of a metal triangle capped by a selenium atom and bridged on two sides, respectively, by a phosphido ligand and by a benzoyl group both deriving from multiple fragmentation of dppf diselenide and migratory insertion of a Ph ring into a CO ligand. Isomers **2** and **3** present different electrochemical behaviour, the bridged one giving a more complicated voltammetric pattern.

Keywords: Electrochemical behaviour; Crystal structures; Isomeric *nido*-clusters

1. Introduction

In the framework of a research project on the reactivity of phosphine selenides towards Group 8 metal carbonyls [1], we have recently reacted 1,1′-bis(diphenylphosphino)ferrocene diselenide (dppfSe2) with $[Fe_3(CO)_{12}]$ and $[Ru_3(CO)_{12}]$ under the same conditions, affording respectively $[Fe_3(\mu_3\text{-}Se)_2(\mu\text{-}dppf)(CO)_7]$ (**1**) [2] and $[Ru_3(\mu_3\text{-}Se)_2(dppf)(CO)_7]$ (**2**) [3] as the main products. Both clusters, sketched in Scheme 1, belong to the numerous family of the open-triangular phosphine-substituted M_3E_2 *nido* clusters (the cluster core can be also regarded as square pyramidal), which are the primary products of the oxidative attack of two equivalents of P=Se groups to the starting triangular clusters.

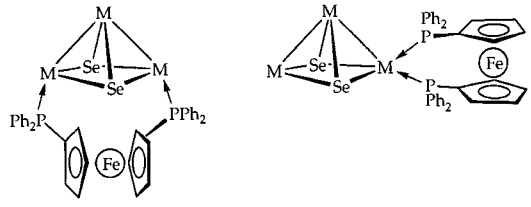

$[Fe_3Se_2(CO)_7(\mu\text{-}dppf)]$ **1**
$[Ru_3Se_2(CO)_7(\mu\text{-}dppf)]$ **3**

$[Ru_3Se_2(CO)_7(dppf)]$ **2**

Scheme 1.

* Corresponding authors. Tel.: +39-521-905-445; fax: +39-521-905-557.
E-mail addresses: predieri@ipruniv.cce.unipr.it (G. Predieri), zanello@unisi.it (P. Zanello).

0022-328X/01/$ - see front matter
PII: S0022-328X(01)00958-5

In compound **1** dppf behaves as bridging ligand as expected, bridging two non bonded iron atoms in the basal plane; by contrast, in cluster **2** the diphosphine adopts a chelating behaviour which was unprecedented for the dppf substituted carbonyl clusters. Both compounds exhibit fluxional behaviour in solution, consisting in the rocking motion of the bidentate bridging ligand below the square basal plane of the iron cluster in **1** and in the exchange of the axial and equatorial positions between the two chelating P atoms in **2**. The dynamic behaviour of both compounds was studied by variable temperature 1D and 2D COSY and EXSY ^{1}H-NMR [3].

Seeking for the bridging ruthenium isomer $[Ru_3(\mu_3\text{-}Se)_2(CO)_7(\mu\text{-dppf})]$ (**3**), we have re-investigated the reaction between dppf diselenide and $Ru_3(CO)_{12}$ and succeeded in obtaining it by changing the thermal conditions. This paper deals with the description of this investigation including the structural characterisations of the new bridged derivative and of the secondary product $[Ru_3Se\{\mu\text{-}P(Ph)C_5H_4FeC_5H_4PPh_2\}(\mu\text{-}OCPh)(CO)_6]$ (**4**) deriving from a P–C(Ph) bond cleavage.

Moreover the availability of the two isomeric clusters **2** and **3** prompted us to study the influence of ligand position on their electrochemical aptitude. In fact, molecules containing redox active multimetallic centres are one of the hot topics in inorganic electrochemistry [4]. In particular, transition metal carbonyl clusters containing redox active ferrocene ligands have attracted much attention in these last years [5].

2. Experimental

2.1. Materials and analytical equipment

The starting reagents $Ru_3(CO)_{12}$, Me_3NO, Se and dppf were pure commercial products (Aldrich and Fluka) and were used as received; 1,1′-bis(diphenylphosphino)ferrocene diselenide ($dppfSe_2$) was prepared according to the literature procedure [2]. The solvents (C. Erba) were dried and distilled by standard techniques before use. All manipulations (prior to the TLC separations) were carried out under dry nitrogen by means of standard Schlenk-tube techniques.

IR spectra (CH_2Cl_2 and toluene solutions) were recorded on a Nicolet 5PC FT spectrometer ^{1}H, ^{31}P (81.0 MHz; 85%-H_3PO_4 as external reference). NMR spectra were recorded for $CHCl_3$-d_1 solutions on Bruker instruments AC 300 (^{1}H) and CXP 200 (^{31}P).

2.2. Reactions

2.2.1. Reaction of $[Ru_3(CO)_{12}]$ with $dppfSe_2$ in refluxing toluene

The reaction of $[Ru_3(CO)_{12}]$ (400 mg, 0.62 mmol) with 445 mg of $dppfSe_2$ (0.62 mmol) and with 46 mg Me_3NO (0.62 mmol) for 3 h in boiling toluene under N_2 gave a deep red solution, which, upon two subsequent TLC purifications on silica (dichloromethane/hexane 1:1 first, and then diethyl ether/hexane 5:2), yielded pure $[Ru_3(\mu_3\text{-}Se)_2(CO)_7(\mu\text{-dppf})]$ (3) (30%) as a red powder, and small amount of other unidentified compounds. Crystallisation of **3** (from CH_2Cl_2–MeOH mixture at 5 °C for some days) gave well-formed crystals of the methanol–water solvate $\mathbf{3}\cdot MeOH\cdot 2H_2O$ suitable for X-ray analysis. Cluster **3**: IR (CH_2Cl_2, νCO, cm^{-1}): 2052vs, 2020s, 2003m, 1987m, 1971m. ^{1}H-NMR ($CHCl_3$-d_1) δ: 3.34 (s, 2H, Cp), 4.01 (s, 2H, Cp), 4.24 (s, 2H, Cp), 4.97 (s, 2H, Cp), 6.8–8.2 (m, 20H, ph). ^{31}P-NMR ($CHCl_3$-d_1) δ: 53.0 (s).

2.2.2. Reaction of $[Ru_3(CO)_{12}]$ with $dppfSe_2$ in toluene at 60 °C

Treatment of $[Ru_3(CO)_{12}]$ (400 mg, 0.62 mmol) with 445 mg of $dppfSe_2$ (0.62 mmol) and with 46 mg Me_3NO (0.62 mmol) for 1.5 h in hot toluene (60°C) under N_2 gave a deep reddish brown solution, which, upon two subsequent TLC purifications on silica, (dichloromethane/hexane 2:1 first, and then diethyl ether/hexane ether 2:1), yielded reddish orange $[Ru_3(\mu_3\text{-}Se)_2(CO)_7(dppf)]$ (**2**) (33%), and small amounts of other unidentified compounds. One of them, $[Ru_3Se\{\mu\text{-}P(Ph)C_5H_4FeC_5H_4PPh_2\}(\mu\text{-}OCPh)(CO)_6]$ (**4**) ($< 1\%$) was identified by solving its crystal structure after careful crystallisation from a dichloromethane–methanol mixture, at 5 °C for some days. Compound **2** was recognised by comparison of its spectroscopic data with those reported in [3]. Cluster **2**: IR (CH_2Cl_2, νCO, cm^{-1}): 2067vs, 2034vs, 1998s, 1986m, 1973m, 1933m. ^{1}H-NMR ($CHCl_3$-d_1) δ: 3.97 (s, 2H, Cp), 4.11 (s, 2H, Cp), 4.34 (s, 2H, Cp), 4.73. (s, 2H, Cp), 7.1–8.0 (m, 20H, ph). ^{31}P-NMR (213 K, $CHCl_3$-d_1) δ: 57.4 (d, axial P) and 40.2 (d, equatorial P).

Cluster **4**: IR (CH_2Cl_2, νCO, cm^{-1}): 2030m, 2012vs, 1985s, 1960sh. ^{1}H-NMR ($CHCl_3$-d_1) δ: 3.97 (s, 1H, Cp), 4.05 (s, 2H, Cp), 4.15 (s, 1H, Cp), 4.35 (s, 1H, Cp), 4.43 (s, 1H, Cp), 4.76. (s, 1H, Cp), 5.08 (s, 1H, Cp), 7.26–7.69 (m, 15H, ph), 7.79–7.88 (m, 5H, benzoyl). ^{31}P-NMR (213 K, $CHCl_3$-d_1) δ: 132.9 (d, $^2J = 22$ Hz, phosphido) and 44.1 (d, $^2J = 22$ Hz).

2.3. Crystal structure determinations of clusters $\mathbf{3}\cdot CH_3OH\cdot 2H_2O$ and **4**

The intensity data of $\mathbf{3}\cdot CH_3OH\cdot 2H_2O$ were collected at room temperature (298 K) on a Bruker AXS Smart 1000, equipped with an area detector diffractometer using a graphite monochromated Mo–K_α radiation. The intensity data of **4** were collected at room temperature (298 K) on a Philips PW 1100 single-crystal dif-

Table 1
Crystal data and structure refinement parameters for **3** $CH_3OH{\cdot}2H_2O$ and **4**

	3·$CH_3OH{\cdot}2H_2O$	**4**
Empirical formula	$Ru_3Se_2FeP_2O_7C_{41}H_{28}$-$CH_3OH{\cdot}2H_2O$	$Ru_3SeFeP_2O_7C_{41}$-H_{28}
Formula weight	1279.73	1132.59
Crystal system	Monoclinic	Monoclinic
Space group	$P2_1/c$	$P2_1/n$
a (Å)	13.492(4)	17.507(4)
b (Å)	17.974(3)	21.635(5)
c (Å)	19.646(5)	10.728(3)
β (°)	105.61(3)	95.99(2)
V (Å^3)	4588(2)	4041(2)
Z	4	4
D_{calcd} (g cm^{-3})	1.852	1.862
$F(000)$	2496	2208
Crystal size	0.18x0.22x0.25	0.21x0.32x0.22
μ (cm^{-1})	29.88	24.80
Reflections collected	26357	12312
Reflections unique	9780 [R(int) = 0.0315]	11755 [R(int) = 0.0410]
Observed reflections	6945 [$I > 2?(I)$]	5886 [$I > 2\sigma(I)$]
Final R indices, [$I > 2\sigma(I)$] [a]	$R_1 = 0.0419$, $wR_2 = 0.1143$	$R_1 = 0.0339$, $wR_2 = 0.0567$
R indices (all data) [a]	$R_1 = 0.0737$, $wR_2 = 0.1343$	$R_1 = 0.1049$, $wR_2 = 0.0709$

[a] $R_1 = \Sigma||F_o|-|F_c||/\Sigma|F_o|$; $wR_2 = [\Sigma[w(F_o^2-F_c^2)^2]/\Sigma[w(F_o^2)^2]]^{1/2}$.

fractometers using a graphite monochromated Mo–K_α radiation and the $\theta/2\theta$ scan technique.

Crystallographic and experimental details for the structures are summarised in Table 1. Corrections for absorption were made for **3**·$CH_3OH{\cdot}2H_2O$, using the Bruker software for absorption correction, and for **4** [maximum and minimum value for the transmission coefficient was 1.000 and 0.620] [6]. The structures were solved by Patterson and Fourier methods and refined by full-matrix least-squares procedures (based on F_o^2) (SHELX-97) [7] first with isotropic thermal parameters and then with anisotropic thermal parameters in the last cycles of refinement for all the non-hydrogen atoms. The hydrogen atoms were introduced into the geometrically calculated positions and refined riding on the corresponding parent atoms, excepting for the carbon and oxygen atoms of the solvent molecules in **3**·$CH_3OH{\cdot}2H_2O$. In the final cycles of refinement a weighting scheme $w = 1/[\sigma^2F_o^2 + (0.0663P)^2 + 9.3845P]$, (**3**·$CH_3OH{\cdot}2H_2O$), and $w = 1/[\sigma^2F_o^2 + (0.0193P)^2]$ (**4**) where $P = (F_o^2 + 2F_c^2)/3$ was used.

The supplementary material for the structures includes the lists of atomic coordinates for the non-H atoms, of calculated coordinates for the hydrogen atoms, of anisotropic thermal parameters and complete lists of bond lengths and angles.

3. Results and discussion

3.1. Preparations and characterisations

In a previous paper [3] we reported that the reaction between dppfSe2 and ruthenium carbonyl in toluene at 70 °C gave, after TLC work-up, a rough product containing the chelate derivative **2** and a small amount of an unidentified compound showing a ^{31}P resonance at δ 53.8. Cluster **2** was purified by fractional recrystallisation, and no attempts were made to characterise the other species. The achievement of the chelate derivative, instead of the bridged one, was unexpected considering that in all the previously reported dppf-substituted carbonyl clusters (including the corresponding triiron diselenido cluster **1**) the bidentate ligand adopted a bridging behaviour. It was proposed on the basis of geometrical considerations, that the chelate behaviour was less favourable for the ruthenium derivative owing to the larger Ru···Ru separation with respect to the iron case.

In order to verify this hypothesis, we have reacted ruthenium carbonyl and dppf under different conditions, in particular at lower (60 °C) and higher temperature (110 °C). In the first case the pure chelate derivative **2** was obtained, whereas in the second one only the bridged cluster **3** was achieved, separated and characterised; the latter displays the same ^{31}P resonance observed for the unidentified compound obtained as a minor species in the reaction at 70 °C. Its ^{1}H-NMR spectrum at room temperature shows four rather sharp peaks, due to the cyclopentadienyl protons (Fig. 1).

This pattern parallels that of the corresponding iron derivative **1** at 273 K [3], indicating that the rocking motion of the ligand, observed for the iron species, suffers in **3** from a higher energy barrier. These results suggest that the bridged cluster (the only isomer attainable at higher temperature) is more stable than the chelate derivative, but its formation requires higher activation energy. On the other hand, the chelate species **2**, which is the more favourable product at lower temperature (under kinetic control) can convert to **3** by simple heating (80 °C) in toluene solution, under CO atmosphere. The conversion, monitored by IR spectroscopy (Fig. 2), is almost complete after 40 h.

Among the minor products present in the reaction mixtures, it was possible to isolate few crystals of the red derivative **4**, which was identified as [Ru_3Se\{μ-

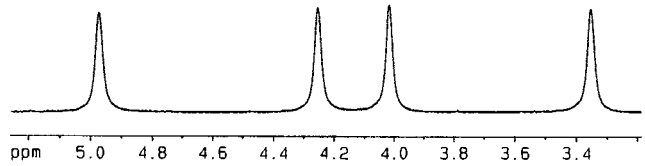

Fig. 1. ^{1}H-NMR spectrum of compound **3**, in the cyclopentadienyl region, recorded at 298 K.

$P(Ph)C_5H_4FeC_5H_4PPh_2\}(\mu\text{-}OCPh)(CO)_6]$ by X-ray structure determination. It derives from the pyrolytic fragmentation of dppf over ruthenium selenido clusters (probably just **2** or **3**) leading to the rupture of a P–C(Ph) bond with formation of bridging phosphido and benzoyl groups. This behaviour parallels that of $[Ru_3(CO)_{10}(dppf)]$, which, by thermolysis in cyclohexane, gives six products formed by cleavages of C–H, P–C(f ring) and P–C(Ph) bonds [8]. Differently from **2** and **3**, the ferrocenyl moiety in cluster **4** appears rather rigid in solution, as its ^{1}H-NMR spectrum at room temperature shows seven sharp peaks due to the eight Cp protons (incidentally two of them have the same chemical shift).

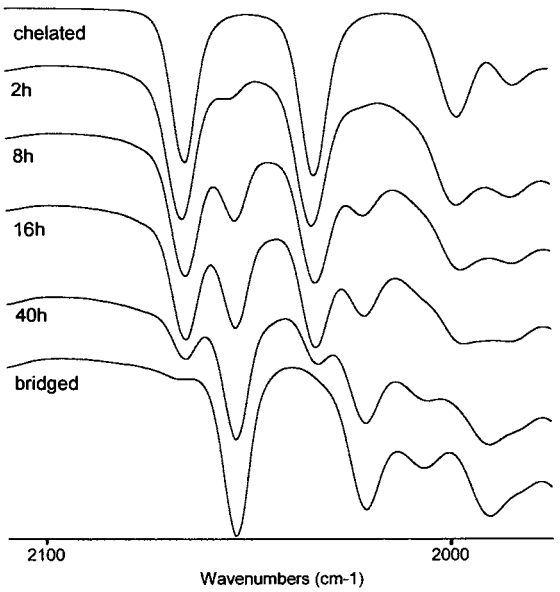

Fig. 2. Temporal evolution of the FT-IR spectrum (in the CO stretching region) of the dppf-chelated cluster **2** (top pattern) in toluene, at 353 K, under CO atmosphere, emphasizing the progressive transformation into the bridged derivative **3** (bottom pattern).

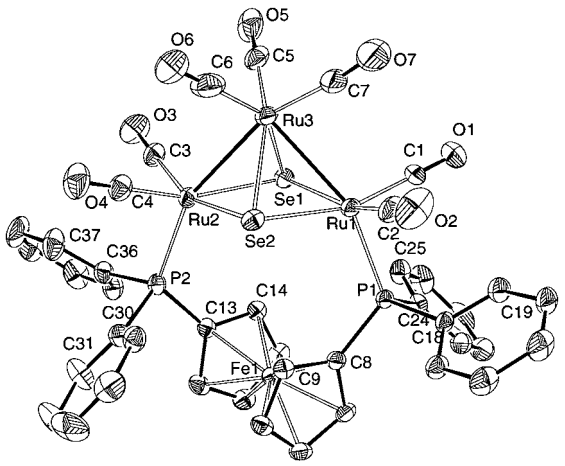

Fig. 3. View of the molecular structure of cluster **3** $[Ru_3Se_2(CO)_7(\mu\text{-}dppf)]$ with the atomic labelling scheme. The thermal ellipsoids are drawn at the 30% probability level.

Table 2
Selected bond lengths (Å) and bond angles (°) for **3**·CH_3OH·$2H_2O$

Bond lengths			
Ru(1)–Ru(3)	2.822(1)	Ru(3)–Se(2)	2.535(1)
Ru(2)–Ru(3)	2.782(1)	Ru(1)–P(1)	2.309(2)
Ru(1)–Se(1)	2.497(1)	Ru(2)–P(2)	2.331(2)
Ru(1)–Se(2)	2.497(1)	Fe(1)–M(1)	1.643(6)
Ru(2)–Se(1)	2.513(1)	Fe(1)–M(2)	1.651(6)
Ru(2)–Se(2)	2.514(1)	P(1)–C(8)	1.808(6)
Ru(3)–Se(1)	2.528(1)	P(2)–C(13)	1.810(7)
Bond angles			
Ru(2)–Ru(3)–Ru(1)	86.14(2)	Se(1)–Ru(3)–Ru(1)	55.30(2)
Ru(1)–Se(1)–Ru(2)	99.62(3)	Se(2)–Ru(3)–Ru(1)	55.24(3)
Ru(1)–Se(2)–Ru(2)	99.61(3)	P(1)–Ru(1)–Ru(3)	156.88(5)
Se(1)–Ru(1)–Se(2)	80.53(3)	P(2)–Ru(2)–Ru(3)	157.60(5)
Se(1)–Ru(2)–Se(2)	79.89(3)	M(1)–Fe(1)–M(2)	175.1(2)
Se(1)–Ru(3)–Se(2)	79.21(3)	C(8)–P(1)–Ru(1)	120.0(2)
Se(1)–Ru(1)–Ru(3)	56.35(2)	C(13)–P(2)–Ru(2)	119.2(2)
Se(2)–Ru(1)–Ru(3)	56.53(3)	C(9)–C(8)–P(1)	127.5(5)
Se(1)–Ru(2)–Ru(3)	56.76(3)	C(12)–C(8)–P(1)	125.6(5)
Se(2)–Ru(2)–Ru(3)	56.94(3)	C(14)–C(13)–P(2)	126.2(5)
Se(1)–Ru(3)–Ru(2)	56.26(3)	C(17)–C(13)–P(2)	126.7(5)
Se(2)–Ru(3)–Ru(2)	56.20(2)		

M(1) is the centroid of the Cp ring C(8) C(9) C(10) C(11) C(12). M(2) is the centroid of the Cp ring C(13) C(14) C(15) C(16) C(17).

3.2. Crystal structures

A view of the structure of **3** is shown in Fig. 3 together with atomic numbering scheme; selected bond distances and angles are given in Table 2. This cluster has the well-known bicapped open triangular core and should be regarded as a *nido*-cluster with seven skeletal electron pairs. The structure of this compound could also be described as a square pyramid with two ruthenium and two selenium atoms alternating in the basal plane and the third ruthenium atom at the apex of the pyramid. The ligand dppf bridges the two unbonded ruthenium atoms at the base of the pyramid in axial position and seven terminal carbonyl groups complete the coordination around the ruthenium atoms. This structure is quite similar to that found for the iron analogue **1** [2]. The four atoms that define the base of the pyramid present distortions from planarity, the two selenium atoms being directed slightly towards the apical ruthenium atom. The two phosphorous atoms are essentially coplanar with the three ruthenium atoms [maximum deviation from the mean plane passing through the five atoms 0.31(2) Å for P(2)], and also the iron atom of the ferrocene group is coplanar [0.057(1) Å]. The ligand dppf causes the same extent of distortion on the geometry of the cluster core observed in **1**. The Ru(1)–Ru(3)–Ru(2) and Se(1)–Ru(3)–Se(2) bond angles [86.14(2) and 79.21(3)°] are in good agreement with those observed in **1** [86.54(6) and 79.14(5)°, respectively]. The coordination demand drives the conforma-

tion of the two Cp rings producing a dihedral angle between the planes defined by P(1), M(1), Fe(1) and P(2), M(2), Fe(1) [M(1,2) = Cp centroids] of 84.1(3)°. This value is slightly larger than that observed in **1** (80°), probably as a consequence of the Ru···Ru distance of 3.83 Å, which is significantly longer than that observed for the iron species (3.63 Å), so requiring a larger P···P separation. This conformation is favourable to promote two short C–H···Se contacts [Se(1)···H(14) 2.703(1) Å, Se(2)···H(9) 2.757(1) Å], as in the case of **1**. The solvent molecules CH_3OH and H_2O present some H-bond interactions, being 2.51(2) and 2.52(2) Å the values of the distances O(2S)···O(1S) and O(3S)···O(1S), respectively.

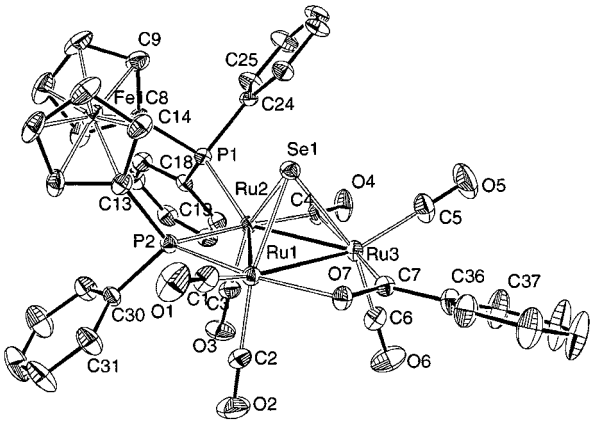

Fig. 4. View of the molecular structure of cluster **4** [$Ru_3Se\{\mu$-$P(Ph)C_5H_4FeC_5H_4PPh_2\}(\mu$-OCPh)$(CO)_6$] with the atomic labelling scheme. The thermal ellipsoids are drawn at the 30% probability level.

Table 3
Selected bond lengths (Å) and bond angles (°) for **4**

Bond lengths			
Ru(1)–Ru(3)	2.812(1)	Ru(2)–C(4)	1.972(4)
Ru(1)–Ru(2)	2.846(1)	Ru(3)–C(4)	2.512(4)
Ru(2)–Ru(3)	2.712(1)	Ru(3)–C(7)	1.995(4)
Ru(1)–Se(1)	2.530(1)	Ru(1)–O(7)	2.234(3)
Ru(2)–Se(1)	2.569(1)	Fe(1)–M(1)	1.643(1)
Ru(3)–Se(1)	2.493(1)	Fe(1)–M(2)	1.649(1)
Ru(1)–P(2)	2.278(1)	O(7)–C(7)	1.238(4)
Ru(2)–P(2)	2.328(1)	C(7)–C(36)	1.499(5)
Ru(2)–P(1)	2.376(1)		
Bond angles			
Ru(3)–Ru(1)–Ru(2)	57.27(1)	M(1)–Fe(1)–M(2)	177.7(2)
Ru(3)–Ru(2)–Ru(1)	60.73(2)	C(8)–P(1)–Ru(2)	121.4(1)
Ru(2)–Ru(3)–Ru(1)	62.0(2)	Ru(1)–P(2)–Ru(2)	76.31(4)
Ru(3)–Se(1)–Ru(1)	68.05(2)	C(7)–O(7)–Ru(1)	110.0(2)
Ru(3)–Se(1)–Ru(2)	64.76(2)	Ru(2)–C(4)–Ru(3)	73.3(1)
Ru(1)–Se(1)–Ru(2)	67.85(2)	O(7)–C(7)–C(36)	115.5(4)
Se(1)–Ru(1)–Ru(3)	55.33(2)	O(7)–C(7)–Ru(3)	113.5(3)
Se(1)–Ru(1)–Ru(2)	56.74(2)	C(36)–C(7)–Ru(3)	131.1(3)
Se(1)–Ru(2)–Ru(3)	56.25(2)	C(9)–C(8)–P(1)	124.8(4)
Se(1)–Ru(2)–Ru(1)	55.41(2)	C(12)–C(8)–P(1)	128.9(3)
Se(1)–Ru(3)–Ru(2)	58.99(2)	C(14)–C(13)–P(2)	128.4(3)
Se(1)–Ru(3)–Ru(1)	56.59(2)	C(17)–C(13)–P(2)	125.0(4)
P(2)–Ru(2)–P(1)	97.5(1)		

M(1) is the centroid of the Cp ring C(8) C(9) C(10) C(11) C(12).M(2) is the centroid of the Cp ring C(13) C(14) C(15) C(16) C(17).

A view of the structure of **4** is shown in Fig. 4 together with atomic numbering scheme; selected bond distances and angles are given in Table 3. It consists of a trinuclear cluster with a Ru_3Se core. The selenium atom caps the metal triangle, two sides of which are bridged by a phosphide and a benzoyl group which derive from the multiple fragmentation of the parent bis-diphenylphosphinoferrocene selenide, followed by the migratory insertion of a phenyl ring into a carbonyl group. The two bridged sides of the metal triangle are the longest ones [2.846(1) and 2.812(1) Å]. On the shortest side [2.712(1) Å] a semibridging carbonyl [Ru(2)–C(4) 1.972(4), Ru(3)–C(4) 2.512(4) Å, Ru(2)–C(4)–O(4) 162.2(4)°] is attached. The three Ru–Se bond distances that span from 2.493(1) to 2.569(1) Å are in good agreement with those observed for Ru_3Se core clusters [9]. As a consequence, the selenido ligand, capping the three metal atoms, is elevated over the plane of the triangle of 1.950(1) Å.

Due to the loss of a phenyl ring, the phosphino–phosphido ligand is coordinated to the Ru(1)–Ru(2) side in an unusual manner: the phosphido atom P(2) both bridges asymmetrically Ru(2) and Ru(1) [P(2)–Ru(1) 2.278(1), P(2)Ru(2) 2.328(1) Å] and participates with P(1) to the chelation of Ru(2) [Ru(2)–P(1) 2.376(1), Ru(2)–P(2) 2.328(1) Å]. The conformation of the two Cp rings is quasi-staggered, being 19.3(2)° the dihedral angle between the planes defined by P(1)M(1)Fe(1) and P(2)M(2)Fe(1). The three metal atoms, C(7), O(7) and P(2) are nearly coplanar [maximum deviation for P(2) 0.82(1) Å]. The P(1) atom and the entire ferrocenyl group are deviated from the same side of the Se ligand.

The migratory insertion of a phenyl ring into the C(7)–O(7) carbonyl group causes the formation of a benzoyl ligand which bridges Ru(3) and Ru(1) in a μ_2-η^1:η^1-fashion respectively through C(7) and O(7). The dihedral angle between the phenyl ring and the mean plane defined by Ru(1)Ru(3)C(7)O(7) is of 20.8(1)°. Only two examples of a μ_2-benzoyl groups bridging two ruthenium atoms in the same μ_2-η^1:η^1-fashion are known [10,11] and there are few examples in literature of benzoyl groups similarly bridging other transition metals, namely Re [12], Os [13], Mn [14], Fe–Re [15] (see Table 4). Other examples quoted Table 4 are relevant to ruthenium compounds where the benzoyl ligand is subjected to other coordinative interactions besides the simple bridge depicted below the Table.

As shown in Table 4, the C(7)–O(7) bond distance 1.238(4) Å is shorter than those found in related compounds but longer than that observed for non-bridging σ-bonded benzoyl unit [1.201(5) Å] [11]. Moreover, the

Table 4
Comparison between bond distances in different compounds containing the bridging ligand PhCO as depicted in the scheme below

	M1–O	M2–C	O–C	M1–M2	Reference and CCD ref. code
M1 = M2 = Ru	2.234(3)	1.995(4)	1.238(4)	2.812(1)	This paper
M1 = M2 = Ru	2.158(2)	2.082(2)	1.262(3)	2.750(1)	[10] DIBSEM
M1 = M2 = Ru	2.170(6)	2.033(8)	1.280(10)	2.783(1)	[11] JODKIW
M1 = M2 = Re	2.191(1)	2.172(2)	1.24(4)	3.122(2)	[12] SIDNOI
M1 = M2 = Os	2.13(1)	2.05(2)	1.29(2)	2.918(1)	[13] YEFCOB
M1 = M2 = Mn	2.06(1)	2.03(1)	1.29(2)	3.006(3)	[14] JOPBOF
M1 = Re, M2 = Fe	2.153(4)	2.002(6)	1.252(7)	2.841(1)	[15] VIVNET
M1 = M2 = Ru	2.145(2)	2.067(4)	1.249(4)	–	[11] JODKIW [a]
M1 = M2 = Ru	2.22(1)	1.98(2)	1.26(2)	2.848(2)	[16] NAJVEZ [b]
M1 = M2 = Ru	2.096(3)	2.059(4)	1.368(5)	2.752(4)	[17] YUNCIT [c]
M1 = M2 = Ru	2.09(2)	2.04(2)	1.40(3)	2.918(3)	[18] PEDRAR [d]

[a] μ_2-COPh on non-bonded Ru···Ru.
[b] μ_2-η^1:η^2-COPh.
[c] μ_3-σ:σ:η^2-COPh.
[d] μ_3-COPh.

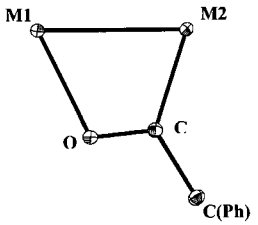

Ru(3)–C(7) [1.995(4) Å] and Ru(2)–O(7) [2.234(3) Å] bond distances are, respectively, significantly shorter and longer than those found in related Ru compounds containing the same μ^2-benzoyl group. This suggests for cluster **4** a certain contribution from a carbene Ru=C(Ph)–O^- form to the bonding. The angles around C(7) are: Ru(3)–C(7)–O(7) 113.5(3), Ru(3)–C(7)–C(36) 131.1(3), C(36)–C(7)–O(7) 115.5(4)°.

3.3. Electrochemistry

Before illustrating the electrochemical behaviour of **2** and **3**, it could be useful to recall that in dichloromethane solution the similar cluster $Ru_3Se_2(CO)_7(PPh_3)_2$ undergoes either an irreversible multielectron oxidation or an irreversible multielectron reduction. On the other hand, dppf exhibits a first ferrocene-centred oxidation, which is accompanied by slow chemical complications [19], and a further irreversible two-electron oxidation centred on the two phosphine subunits.

This being stated, Fig. 5a,b compares the cyclic voltammetric behaviour of **2** with that of **3**. A helpful insight into the redox pathway can be also given by the voltammetric profile of $Ru_3Se_2(CO)_7$(μ-dppm), Fig. 5c.

Cluster **2** exhibits a first irreversible oxidation and an irreversible reduction which, because of their similarity to those of $Ru_3Se_2(CO)_7(PPh_3)_2$, are both assigned to processes centred on the $Ru_3Se_2(CO)_7$ core. A further anodic step with features of chemical reversibility is also present which is conceivably assigned to the oxidation of the dppf ligand. Based on the relative peak heights, the oxidation of the $Ru_3Se_2(CO)_7$ fragments looks like a two-electron process. As shown in Table 5, which quotes the relevant electrode potentials, no significant electronic perturbation arises inside the $Ru_3Se_2(CO)_7$ core from the assembly with the dppf ligand, even if the slight splitting of the cathodic process, as we will discuss below, deserves attention. By contrast, the dppf ligand appears significantly affected in that the first electron removal is made more difficult by 0.35 V and the second phosphine-centred oxidation is shifted beyond the solvent discharge.

A somewhat more complicated voltammetric pattern is exhibited by the bridged derivative **3** with respect to the preceding profile of its isomer **2**, as a third oxidation appears possessing features of partial chemical reversibility. In addition, the reduction process is now completely split in two successive steps, the most cathodic one displaying partial chemical reversibility. From a qualitative viewpoint the appearance of the third oxidation can be attributed either to the cited oxidation of the phosphine groups of the dppf ligand, or to the fact that the dppf bridge, either limiting the occurrence of severe geometrical reorganisations of the Ru_3Se_2 core or rendering communicating two Ru centres, allows it to lose electrons through separate sequences. The Ru_3Se_2-centred attribution is supported by the fact that, because of the coordination to the

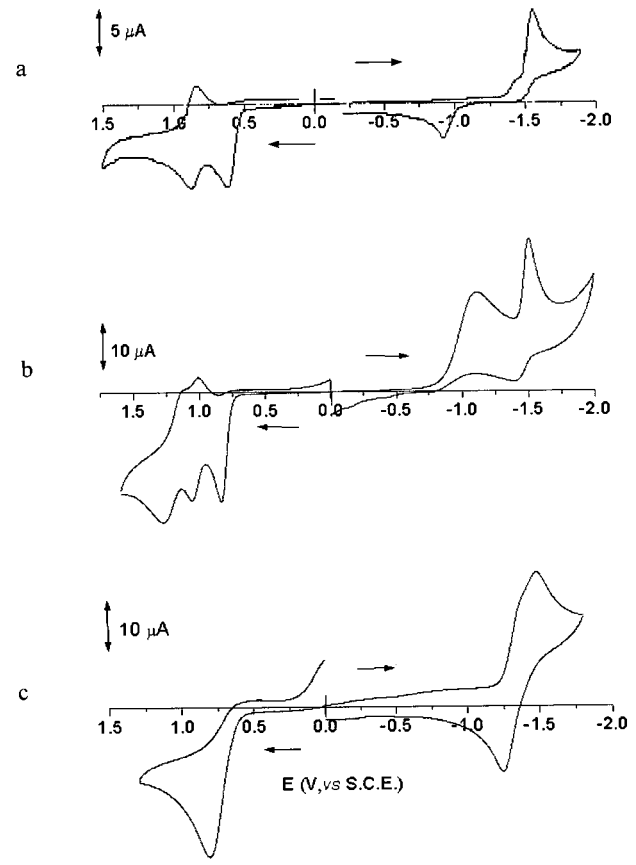

Fig. 5. Cyclic voltammograms recorded at a platinum electrode on CH_2Cl_2 solutions of: (a) $[Ru_3Se_2(CO)_7(dppf)]$ (0.6×10^{-3} mol dm^{-3}); (b) $[Ru_3Se_2(CO)_7(\mu\text{-dppf})]$ (0.9×10^{-3} mol dm^{-3}); (c) $[Ru_3Se_2(CO)_7(\mu\text{-dppm})]$ (1.0×10^{-3} mol dm^{-3}). $[NBu_4][PF_6]$ (0.2 mol dm^{-3}) supporting electrolyte. Scan rate 0.2 V s^{-1}.

metal fragment, the second oxidation of dppf is expected to shift towards more positive values (substantially beyond the solvent discharge), as it happens for the first oxidation, which is shifted by about 0.4–0.5 V with respect to free dppf. We favour the last hypothesis even if it is not apparently supported by the behaviour of $Ru_3Se_2(CO)_7(\mu\text{-dppm})$, which exhibits a single oxidation process; nevertheless, its reduction step is slightly split. In this connection, it must be taken into account that it is well conceivable that the dppf and dppm bridges possess different electronically connecting abilities. On the other hand, the beneficial cohesive effects of coordinating polyphosphines towards redox changes in metal–carbonyl clusters is nicely proved by the behaviour of $Co_4(CO)_9[HC(PPh_2)_3]$, which displays multiple reversible one-electron exchanges, whereas unsubstituted $Co_4(CO)_{12}$ exhibits a single one-electron reduction complicated by slow chemical reactions [21].

As Fig. 6b illustrates, the anodic behaviour exhibited by **1** is apparently similar to that of **3**. As a matter of fact, the parent cluster $Fe_3Se_2(CO)_9$ (Fig. 6a) exhibits a first, partially chemically reversible one-electron reduction ($i_{pa}/i_{pc} = 0.8$ at 0.2 V s^{-1}), followed by a second irreversible reduction, as well as an irreversible two electron oxidation. In this light, the anodic path of **1** is interpreted as follows: in analogy with **3**, the second electron removal is attributed to the bridging ferrocene unit, whereas the first and third steps are assigned to the Fe_3Se_2 core, which, because of the communicating constraint of the ferrocene diphosphine, is oxidised in two separate steps. Indeed, the fact that the first oxidation might be centred on the ferrocene ligand cannot be

Table 5
Formal electrode potentials (V, vs. SCE) and peak-to-peak separations (mV) for the redox changes exhibited by the M_3Se_2 (M = Ru, Fe) clusters under study in dichloromethane solution

Complex	Oxidation processes						Reduction processes		
	$E^{\circ\prime}$	ΔE_p [a]	$E^{\circ\prime}$	ΔE_p [a]	$E^{\circ\prime}$	ΔE_p [a]	$E^{\circ\prime}$	ΔE_p [a]	E_p
$Ru_3Se_2(CO)_7(PPh_3)_2$					+0.72 [a,b]		−1.53 [a,b]		
$Ru_3Se_2(CO)_7(dppf)$			+0.93	42	+0.73 [a,b]		−1.52 [a,b,d]		
$Ru_3Se_2(CO)_7(\mu\text{-dppm})$					+0.82 [a,b]		−1.15	210	
$Ru_3Se_2(CO)_7(\mu\text{-dppf})$	+1.29 [a,b]	160	+1.04	58	+0.84 [a,b]		−1.12 [a,b]		−1.45 [c]
dppf	+1.38 [a,b]	–	+0.58	80					
$Fe_3Se_2(CO)_9$	+1.30 [a,b,e]	–					−0.67	82	−1.35
							−0.56 [f]	100 [f]	–
$Fe_3Se_2(CO)_7(\mu\text{-dppf})$	+1.28 [a,b]	80	+0.98	83	+0.73	75	−1.12	90	−2.0 [g]
FcH			+0.40	92					

[a] Measured at 0.2 V s^{-1}
[b] Peak potential.
[c] Affected by electrode adsorption.
[d] Partially splitted in two processes.
[e] Multielectron process.
[f] From Ref. [20].
[g] Scarcely detected.

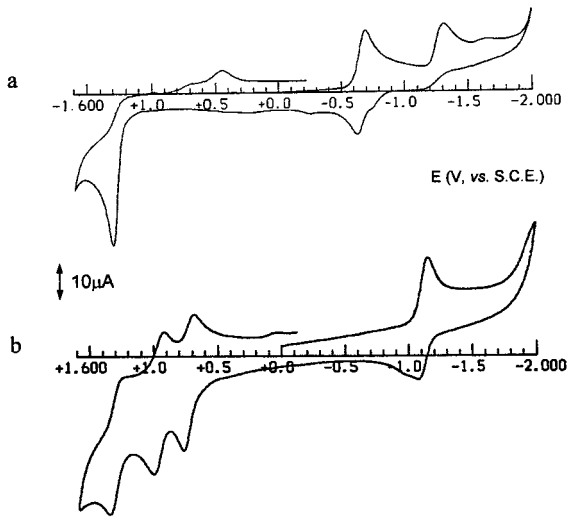

Fig. 6. Cyclic voltammograms recorded at a platinum electrode on CH_2Cl_2 solutions of: (a) $[Fe_3Se_2(CO)_9]$ (1.1×10^{-3} mol dm^{-3}); (b) $[Fe_3Se_2(CO)_7(\mu\text{-dppf})]$ (1.0×10^{-3} mol dm^{-3}). $[NBu_4][PF_6]$ (0.2 mol dm^{-3}) supporting electrolyte. Scan rate 0.2 V s^{-1}.

ruled out; unfortunately we could not ascertain spectroscopically the nature of this process in that exhaustive one-electron oxidation by controlled potential coulometry led to complete decomposition of the cluster monocation.

As far as the cathodic behaviour is concerned, in this case the bridging dppf adds electron density to the Fe_3Se_2 core greater than to Ru_3Se_2, making the reduction processes significantly more difficult by about 0.5 V.

In conclusion, we have proved that the insertion of the redox-active dppf in bridging position notably increases the electron mobility inside cluster assemblies.

4. Supplementary material

Crystallographic data for the structural analysis have been deposited with the Cambridge Crystallographic Data Centre, CCDC Nos. 157527 for compound **3**·CH_3OH·$2H_2O$ and 157526 for compound **4**. Copies of this information may be obtained free of charge from The Director, CCDC, 12 Union Road, Cambridge CB2 1EZ, UK (fax: +44-1233-336-033; e-mail: deposit@ccdc.cam.ac.uk or www: http://www.ccdc.cam.ac.uk).

Acknowledgements

Financial support from Ministero dell'Università e della Ricerca scientifica e Tecnologica (Rome, Cofin 2000) is gratefully acknowledged. The facilities of the Centro Interdipartimentale di Misure 'G. Casnati' (Università di Parma) were used to record the NMR and mass spectra.

References

[1] D. Cauzzi, C. Graiff, G. Predieri, A. Tiripicchio, in: P. Braunstein, L. Oro, P. Raithby (Eds.), Metal Cluster in Chemistry, vol. 1, VCH, Weinheim, 1999, p. 193.
[2] D. Cauzzi, C. Graiff, M. Lanfranchi, G. Predieri, A. Tiripicchio, J. Organomet. Chem. 536–537 (1997) 497.
[3] D. Cauzzi, C. Graiff, C. Massera, G. Predieri, A. Tiripicchio, D. Acquotti, J. Chem. Soc. Dalton Trans. (1999) 3515.
[4] See for instance: W. Kaim, A. Klein, M. Glöckle, Acc. Chem. Res. 33 (2000) 755 and references therein.
[5] (a) P. Zanello, in: T. Hayashi, A. Togni (Eds.), Ferrocenes. From Homogeneous Catalysis to Material Science, Ch. 7, VCH, Weinheim, 1995;
(b) Updated references: Ruthenium complexes: A.J. Blake, A. Harrison, B.F.G. Johnson, E.J.L. McInnes, S. Parsons, D.S. Shephard, L.J. Yellowlees, Organometallics 14 (1995) 3160;
(c) W.-Y. Wong W.-T. Wong, J. Chem. Soc. Dalton Trans. (1996) 3209;
(d) C.S.-W. Lau, W.-T. Wong, J. Organomet. Chem. 588 (1999) 113;
(e) Osmium complexes: S.-M. Lee, K.-K. Cheung, W.-T. Wong, J. Organomet. Chem. 506 (1996) 77;
(f) L.P. Clarke, J.E. Davies, P.R. Raithby, G.P. Shields, J. Chem. Soc. Dalton Trans. (1996) 4147;
(g) S.L. Ingham, B.F.G. Johnson, P.R. Raithby, K.J. Taylor, L.J. Yellowlees, J. Chem. Soc. Dalton Trans. (1996) 3521;
(h) J.W.-S. Hui, W.-T. Wong, J. Chem. Soc. Dalton Trans. (1997) 2445;
(i) R.D. Adams, B. Qu, Organometallics 19 (2000) 2411;
(j) R.D. Adams, B. Qu, Organometallics 19 (2000) 4090;
(k) Cobalt complexes: H. Shen, S.G. Bott, M.G. Richmond, Inorg. Chim. Acta 250 (1996) 195;
(l) S. Onaka, H. Muto, Y. Katsukawa, S. Takagi, J. Organomet. Chem. 543 (1997) 241.
[6] (a) N. Walker, D. Stuart, Acta Crystallogr. Sect. A 39 (1983) 158;
(b) F. Ugozzoli, Comput. Chem. 11 (1987) 109.
[7] G.M. Sheldrick, 'SHELX-97', Program for the Solution and the Refinement of Crystal Structures, Universität Göttingen, Germany, 1997.
[8] M.I. Bruce, P.A. Humphrey, O. b. Shawkataly, M.R. Snow, E.R.T. Tiekink, W.R. Cullen, Organometallics 9 (1990) 2910.
[9] D. Cauzzi, C. Graiff, C. Massera, G. Predieri, A. Tiripicchio, Inorg. Chim. Acta 300-302 (2000) 471.
[10] A. Basu, S. Bhaduri, H. Khwaja, P.G. Jones, T. Schroeder, G.M. Sheldrick, J. Organomet. Chem. 290 (1985) C19.
[11] J.P.H. Charmant, H.A.A. Dickson, N.J. Grist, J.B. Keister, S.A.R. Knox, D.A.V. Morton, A.G. Orpen, J.M. Vinas, Chem. Commun. (1991) 1393.
[12] H.-J. Haupt, C. Heinekamp, U. Florke, Inorg. Chem. 29 (1990) 2955.
[13] C.J. Adams, M.I. Bruce, P.A. Duckworth, P.A. Humphrey, O. Kuhl, E.R.T. Tiekink, W.R. Cullen, P. Braunstein, S.C. Cea, B.W. Skelton, A.H. White, J. Organomet. Chem. 467 (1994) 251.
[14] H.-J. Haupt, C. Heinekamp, U. Florke, U. Juptner, Z. Anorg. Allg. Chem. 608 (1992) 100.
[15] D. Xu, H.D. Kaesz, S.I. Khan, Inorg. Chem. 30 (1991) 1341.

[16] J.A. Cabeza, I. del Rio, V. Riera, S. Garcia-Granda, S.B. Sanni, Organometallics 16 (1997) 1743.
[17] A.J. Blake, P.J. Dyson, B.F.G. Johnson, C.M. Martin, J. Organomet. Chem. 492 (1995) C17.
[18] C.J. Adams, M.I. Bruce, O. Kuhl, B.W. Skelton, A.H. White, J. Organomet. Chem. 445 (1993) C6.
[19] G. Pilloni, B. Longato, B. Corain, J. Organomet.Chem. 57 (1991) 420.
[20] T.M. Bockman, J.K. Kochi, J. Am. Chem. Soc. 109 (1987) 7725.
[21] G.F. Holland, D.E. Ellis, W.C. Trogler, J. Am. Chem. Soc. 108 (1986) 1884.